**JQS** ## Journal of Quaternary Science                    **QRA**

# LakeCC: a tool for efficiently identifying lake basins with application to palaeogeographic reconstructions of North America

SEBASTIAN HINCK,[1]* (iD) EVAN J. GOWAN[1,2] (iD) and GERRIT LOHMANN[1,2] (iD)
[1]Alfred Wegener Institute Helmholtz Centre for Polar and Marine Research, Bremerhaven, Germany
[2]MARUM – Center for Marine Environmental Sciences, University Bremen, Bremen, Germany

ABSTRACT: Along the margins of continental ice sheets, lakes formed in isostatically depressed basins during glacial retreat. Their shorelines and extent are sensitive to the ice margin and the glacial history of the region. Proglacial lakes, in turn, also impact the glacial isostatic adjustment due to loading, and ice dynamics by posing a marine-like boundary condition at the ice margin. In this study we present a tool that efficiently identifies lake basins and the corresponding maximum water level for a given ice sheet and topography reconstruction. This algorithm, called the LakeCC model, iteratively checks the whole map for a set of increasing water levels and fills isolated basins until they overflow into the ocean. We apply it to the present-day Great Lakes and the results show good agreement (∼1–4%) with measured lake volume and depth. We then apply it to two topography reconstructions of North America between the Last Glacial Maximum and the present. The model successfully reconstructs glacial lakes such as Lake Agassiz, Lake McConnell and the predecessors of the Great Lakes. LakeCC can be used to judge the quality of ice sheet reconstructions. © 2019 The Authors Journal of Quaternary Science Published by John Wiley & Sons Ltd.

KEYWORDS: glacial lake; Great Lakes; Lake Agassiz; North America; paleogeography

## Introduction

During the retreat of ice sheets, vast amounts of freshwater are released. The retreating ice also leaves a deeply depressed topography that only slowly recovers due to delayed glacial isostatic adjustment (GIA). In this depressed terrain along the ice margin, meltwater accumulates and forms lakes. These can be the size of an inland sea and impose marine-like boundary conditions on the ice sheet (Tweed and Carrivick, 2015), which may impact the ice dynamics. The largest proglacial lake in North America after the Last Glacial Maximum (LGM) was Lake Agassiz, which formed along the southern margin of the Laurentide Ice Sheet (LIS) (Teller and Leverington, 2004). In Europe, when the Fennoscandian Ice Sheet retreated, the Baltic Ice Lake formed in the basin of the Baltic Sea (Björck, 1995). Today, strandlines and lake sediments provide evidence of the extent of these ancient lakes.

Due to retreating ice and ongoing GIA, the basins evolved over time. The opening of a new, lower outlet could lead to the sudden drainage of a proglacial lake. These events can be observed today with lakes next to alpine glaciers (Walder *et al.*, 2006), but it also happened with ancient lakes. One example is the catastrophic drainage of Lake Missoula, that, due to repeated advances and retreats of the ice sheet, filled and drained more than 40 times (Waitt, 1985). These outburst floods eroded the Channeled Scablands in Washington (Bretz, 1923; Pardee, 1942; Waitt, 1985; Hanson *et al.*, 2012).

Many studies have shown the impact of freshwater hosing on ocean circulation and global climate (e.g. Manabe and Stouffer, 1997; Lohmann and Schulz, 2000; Kageyama *et al.*, 2009). In this regard the evolution of proglacial lakes is of particular relevance. Many hypotheses about the causes

of sudden cooling events invoke the (partial) drainage of glacial lakes into the ocean (e.g. Broecker *et al.*, 1989; Barber *et al.*, 1999; Broecker, 2006; Murton *et al.*, 2010; Carlson and Clark, 2012; Wickert, 2016).

The load of the lakes' mass also impacts GIA and should therefore ideally also be considered when reconstructing palaeo ice sheets, as done by Tarasov and Peltier (2006) and Lambeck *et al.* (2010). Although the impact on GIA is relatively small compared to the ice load, this secondary effect will improve the results of palaeogeography reconstructions. By comparing reconstructed lakes with geological data from the field, these can be fine-tuned.

In this study we present the LakeCC model (CC stands for 'connected components') that locates closed basins that would fill with water for given ice and terrain maps. It is applied to reconstructions of the North American ice-complex after the LGM to the present day (PD) from the NAICE (Gowan *et al.*, 2016b) and ICE-6G (Peltier *et al.*, 2015) models. The results of the latter, however, are only briefly discussed here. After a description of the LakeCC model and its application, the results are compared with geological data. Finally, we discuss the results with regard to possible improvements of the ice margins and different drainage scenarios of Lake Agassiz.

## Methodology

### Bed topography

As with most hydrological applications where water is routed through a digital elevation model (DEM), spatial resolution is a critical factor. Narrow spillways can have a significant impact on the results. Increasing resolution might add accuracy but also brings big challenges with regard to computational resources and suitable numerical implementation that is capable of efficiently processing big data (Barnes, 2016).

*Correspondence: S. Hinck, as above.
E-mail: sebastian.hinck@awi.de

Although high resolution might be a critical issue, it might not always be possible to obtain a data set of sufficient quality, especially when using reconstructed palaeo data sets. These data contain relatively large uncertainties in the glacial history and erosion on the Earth's surface. In this study, we use a high-resolution present-day topography map, combined with the reconstructed bed deformation from a GIA model.

The reference PD topography is the RTopo-2 dataset by Schaffer *et al.* (2016), which is a compilation of various topography and bathymetry data sets on a 30 arcsec grid. Lake bathymetry, except the Great Lakes and Lake St. Clair, is missing from this data set. Consequently, other lakes cannot properly be reconstructed. For further processing, the data are remapped onto a lower resolution projected grid: a Lambert azimuthal equal area projection centred at $60°$ N and $94°$ W with a resolution of 5 km. By simply interpolating, sub-grid information about possible spillways would be lost. Therefore, a minimum-filter is applied to the high-resolved grid and the result is subsequently interpolated onto the projected grid. The minimum-filter assigns each cell the height of the lowest cell within a certain distance. It should be noted that this filtered map is only used to determine the lake basins, which are later transferred back to the unfiltered map.

### Ice sheet and bed deformation

To represent the palaeogeography of the North American continent, the NAICE ice sheet reconstruction (Gowan *et al.*, 2016b) is used. The ice sheets are determined using the ICESHEET model (Gowan *et al.*, 2016a), which takes ice margin reconstructions and a model of basal shear stress as inputs and uses simplified ice physics to calculate ice surface elevation. A temporally and spatially varying basal shear stress model is tuned to create a glacial history that fits best with geological and geophysical measurements, such as GIA uplift rates, relative sea level and glacial lake strandline tilts. Gowan *et al.* (2016b) focused mainly on the western LIS. In this region the ice margins are inferred from the minimum timing of retreat given in Gowan (2013). For the eastern LIS and the Cordilleran Ice Sheet (CIS) the ice margins from Dyke (2004) are assumed. The reconstructions of the Innuitian and the Greenland Ice sheet were also obtained using the ICESHEET model by Khosravi (2017). The output of the NAICE model contains maps of the ice thickness and the bed deformation, which are combined with modern topography to produce the palaeogeography.

The proper reconstruction of post-LGM ice distribution and GIA requires estimates of the pre-LGM glacial history which is generally only poorly constrained (Gowan *et al.*, 2016b). The NAICE reconstructions could, for example, be improved by using a more recent compilation of pre-LGM ice constraints (e.g. Batchelor *et al.*, 2019).

### LakeCC

#### Algorithm

Depressions in a DEM act as a sink for many algorithms of flow routing. One possibility to overcome this issue is to remove all depressions from the DEM by filling them (Barnes *et al.*, 2014; Barnes, 2016). Other, even more elaborate methods, create a drainage hierarchy (Barnes *et al.*, 2019). The focus of this study is the identification of lake basins, without including advanced flow routing techniques. The LakeCC model is developed only for this purpose. For some other lake filling methods (e.g. Berends and van de Wal, 2016) a cell within each lake's basin has to be picked to determine its extent and minimum spillway. This is not required in our model. It assesses every lake basin of the domain, which is advantageous to get an overview of a whole map, without selecting individual lakes. The LakeCC model iterates over a set of increasing water levels, similar to the approach described in Wu *et al.* (2015) and Wu and Lane (2016).

The LakeCC algorithm requires a mask that contains information about sinks (i.e. ocean cells or domain margin) of the map. A simple way to do this would be to just set every cell below sea level to be an ocean cell. However, this would also label cells as ocean that are below sea level but inside the continent, and therefore prevent a lake from forming. A more advanced method, called SeaLevelCC, is also implemented into the LakeCC tool box.

Both methods, LakeCC and SeaLevelCC, are based on a simple 4-neighbour connected-component (CC) labelling algorithm, which is efficiently implemented using run-length encoding and union-find strategies (see Fig. 1). It was adapted from a tool written by Khroulev (2017) for identifying icebergs from a mask within the Parallel Ice Sheet Model (PISM) (the PISM authors, 2015). This underlying code iterates through the map and adds cells that satisfy the flooding criterion (Equation (1)) for a given water level $h$ either to an adjacent patch or, if not present, to a new patch.

$$H(i,j) + \frac{\rho_{ice}}{\rho_{water}} T(i,j) < h \qquad (1)$$

Here $H$ is the bedrock elevation, $T$ is the ice thickness and $\rho_{ice}$ and $\rho_{water}$ are the densities of ice and water, respectively. Additionally, if Equation (1) applies, the mask is checked and if
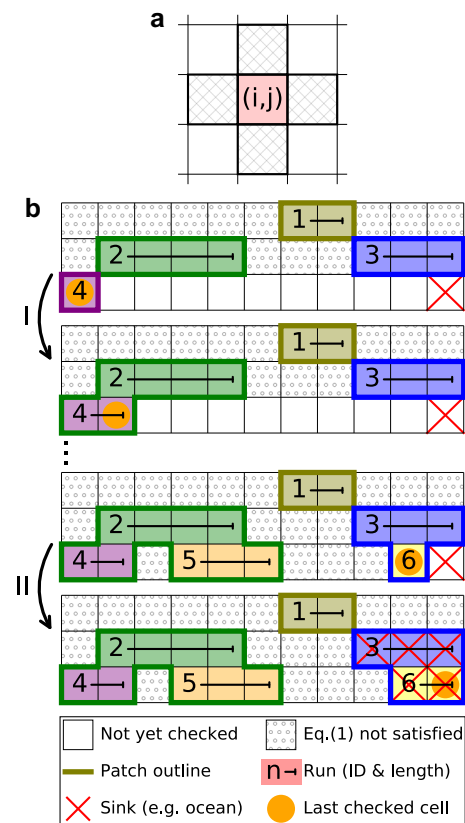


**Figure 1.** (a) In the 4-neighbour connected-component (CC) algorithm only the four direct neighbours along the main grid directions (hatched cells) are considered when checking for connectivity, i.e. diagonal cells are ignored. (b) Schematic of the iteration over the grid. Successive cells within a row that satisfy Equation (1) are merged as runs (identified by an ID, start point and length). Connected runs are merged as patches (see step I), which are identified here by their coloured outline. Step II illustrates the merging of a patch with a sink. [Color figure can be viewed at wileyonlinelibrary.com].

the flooded cell is marked as a sink, the corresponding patch and all associated cells become a sink (see Fig. 1b, step II).

The SeaLevelCC method requires a mask, with cells guaranteed to be ocean marked as sink. If this information is not available, the entire domain's margin can simply be set to sink before applying the CC method at sea level. By doing so the formation of inland ocean basins is effectively inhibited, as ocean patches need to be below sea level and connected to the domain's margin. After the land/sea mask is determined, the LakeCC algorithm is applied, which is shown in Fig. 2. It applies the CC method for a set of increasing water levels $h$. The resulting patches that are not labelled as sink represent a lake basin at the respective level. These patches grow in size as the level rises. Until a patch merges with another one that is a sink, i.e. the lake overflows, the current level $h$ is stored for all associated cells (see blue box in Fig. 2). After this is done for various levels between $h_{min}$ and $h_{max}$, the map contains an estimation of the basins' maximum fill levels within this range. The maximum uncertainty, apart from uncertainties originating from the discretised input topography, depends on the spacing $dh$ between successive levels. For each lake, it is further checked if at least one cell of the lake is ice-free, to prevent sub-glacial lakes from forming.

## Application

Fig. 2 depicts the application of the LakeCC algorithm as a flowchart diagram. The topography map is prepared as described above. Different filter diameters were tested and finally a value of 10 km was chosen as it makes the best compromise between draining under-resolved valleys and retaining realistic lake reconstructions. The domain used in this study is 7755 km x 5955 km, which, at 5 km resolution, is represented by a 1551×1191 rectangular grid. Successive water levels are evenly distributed between 0 and 1800 m by $dh = 0.2$ m.

The minimum-filtered topography map is assumed to retain information about possible spillways as needed for the filling algorithm. For the further steps, a smooth approximation of the actual bed is preferred. The lake levels obtained from the filtered map are transferred back onto the unfiltered map. This is possible since the filtered map represents an over-deepened version of the unfiltered map and therefore lake levels tend to be lower and thus still be valid on the unfiltered map.

The runtime of the LakeCC algorithm depends on the topography and ice configuration. It is shortest when large parts of the map are ice-covered and only a few lakes appear, and longest if many lakes exist in the domain. In our study,
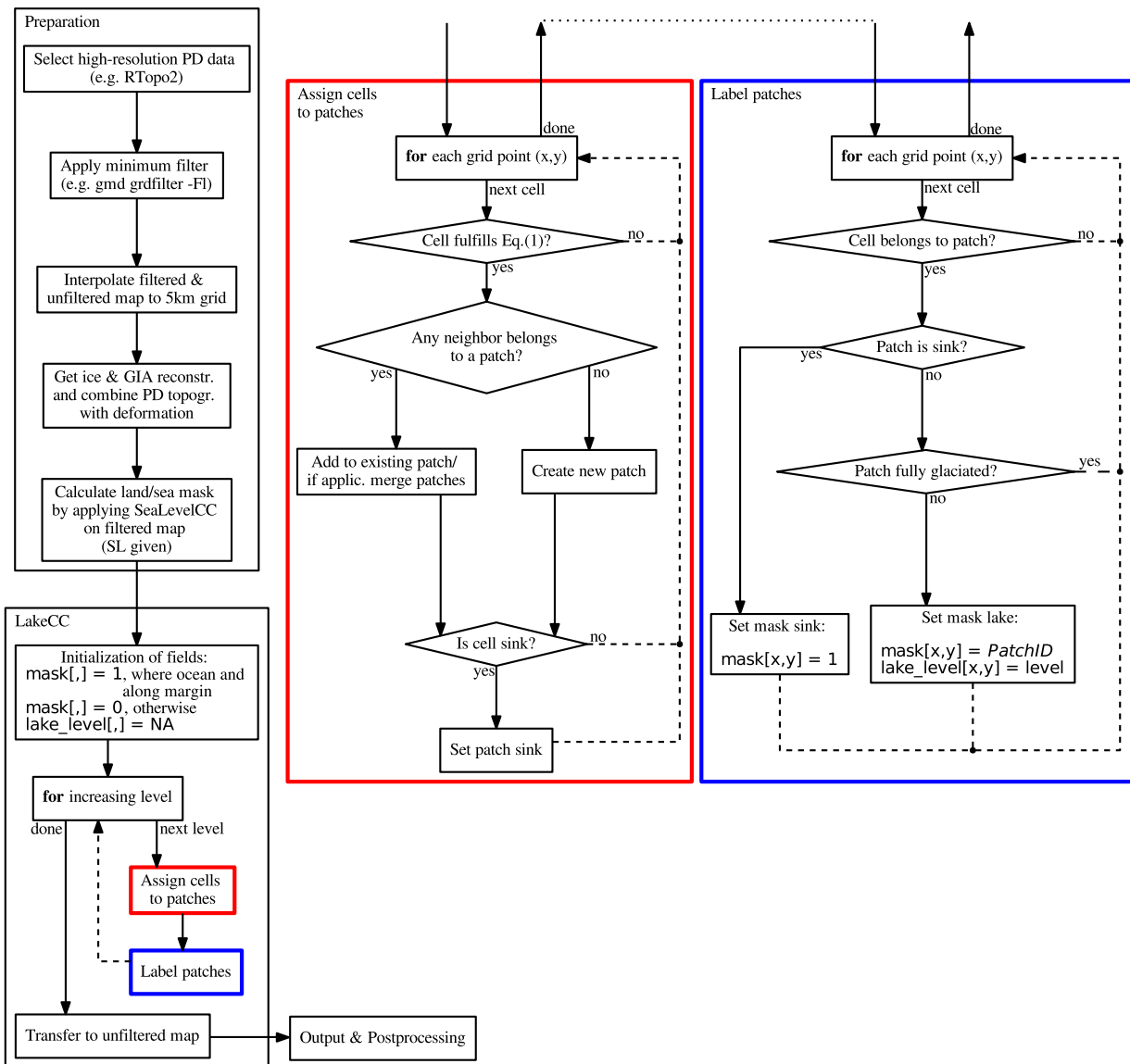


**Figure 2.** Flowchart diagram showing the application of the LakeCC algorithm (left). The red and blue boxes on the right coincide with the respective coloured boxes on the left. For more detail see the main text. [Color figure can be viewed at wileyonlinelibrary.com].

iteration over 9000 different levels took between 250 and 330 s on a 2.4 GHz Intel Xeon processor.

## Post-processing

To get an estimate of the area, volume and maximum depth of certain lakes, another simple algorithm is applied to the output of the LakeCC model. It iterates over the grid and collects this data for all lakes.

In the next step, the map is divided into basins according to the slope of the topography. Each basin is assumed to overflow at its lowest boundary cell into a neighbouring basin. The drainage route is followed until a basin is reached that is marked as a sink (i.e. ocean or domain boundary). To prevent getting stuck in an infinite loop, it checks whether a basin has already been visited and marks the involved basins if necessary. In a subsequent iteration, all labelled basins are checked for the next highest spillway that escapes the loop. After iterating until no loops are left, each basin can be assigned a drainage route into the ocean.

## Results

In this section, the lakes calculated for the different ice sheet reconstructions between the LGM and PD are presented. Some regions of interest are selected and highlighted in the following

subsections. These regions are shown in the overview map (Fig. 3) as black rectangles. Overview maps of the ice- and lake reconstructions on the North American continent between 21 ka BP (Fig. S2A) and PD (Fig. S2V) are provided in S2. Although pre-LGM ice reconstructions are available from the NAICE model (Gowan *et al.*, 2016b) these are not examined, since the ice margins are only poorly constrained. Table S1 gives the lake surface area, volume, water level, maximum depth and the sink (ocean basin where the lake drains to) for all identified lakes for all time slices.

## Great Lakes

During the LGM the southern ice margin of the LIS was south of the Great Lakes, whose basins were fully ice-covered. As ice retreated, parts of the basins were exposed and became proglacial lakes. The reconstruction of glacial lakes in the Great Lakes' basins, including Lakes Maumee, Chicago, Algonquin, Duluth, Chippewa and Stanley, is in good agreement with the literature (Taylor, 1915; Larsen, 1988; Lewis and Anderson, 1989; Lewis *et al.*, 1994; Breckenridge, 2013). Fig. 4 shows some snapshots of this region for different times.

Fig. 5 shows that there is a good match of the PD lake reconstruction with the actual shorelines. Table 1 presents a more quantitative comparison of the lake reconstruction
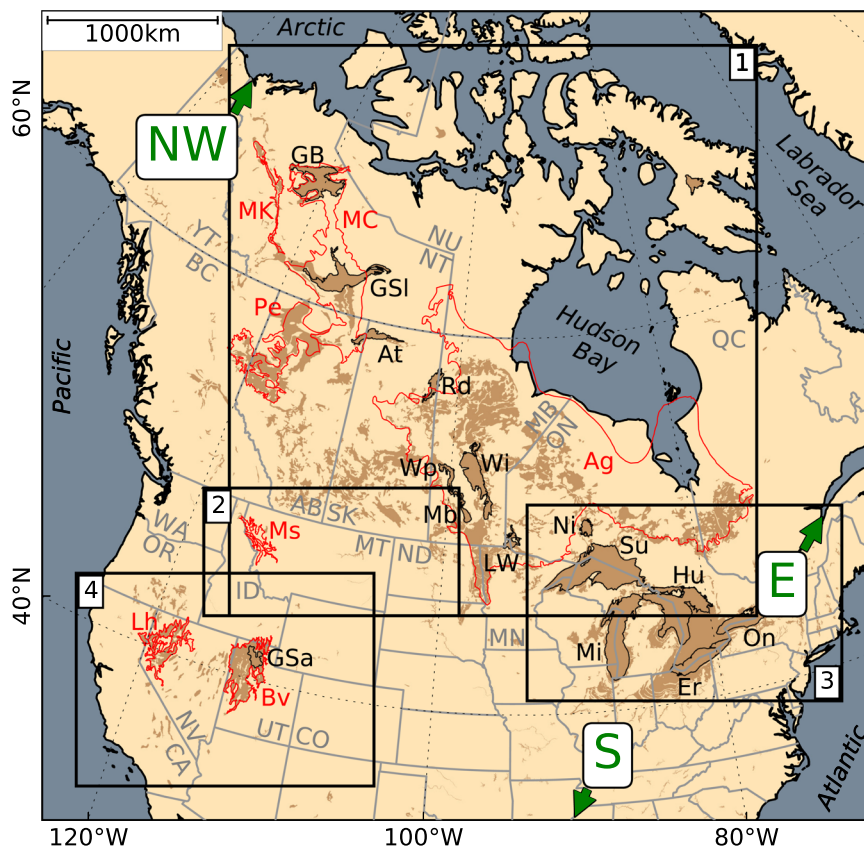


**Figure 3.** Overview of the study site. Black rectangles show the sections of the map focused on in the text: (1) Central North, (2) Montana, (3) Great Lakes and (4) Great Basin. Major PD lakes are shown as thin black outlines with a black label: At – Athabasca; Er – Erie; GB – Great Bear Lake; GSa – Great Salt Lake; GSl – Great Slave Lake; Hu – Huron; LW – Lake of the Woods; Mb – Manitoba; Mi – Michigan; Ni – Nippigon; On – Ontario; Rd – Reindeer; Su – Superior; Wi – Winnipeg; Wp – Winnipegosis. The red outlines represent the basins of major palaeolakes discussed in the paper: Ag – Agassiz (Teller and Leverington, 2004); Bv – Bonneville (Chen and Maloof, 2017); Lh – Lahontan (Reheis, 1999b); MC – McConnell (Smith, 1994); MK – McKenzie (Smith, 1992); Ms – Missoula (Hanson *et al.*, 2012); Pe – Peace (Mathews, 1980; Hickin *et al.*, 2015). Areas where surficial sediments (Fullerton *et al.*, 2003; Soller *et al.*, 2009; Geological Survey of Canada, 2014) indicate a lacustrine history are shown in brown. The green arrows depict likely drainage routes of Lake Agassiz that are discussed in the text: E – eastern drainage via St. Lawrence River; NW – northwestern drainage via the McKenzie River; S – southern drainage via the Mississippi River. Furthermore, the following Canadian and U.S. American states are labelled in grey: AB – Alberta; BC – British Columbia; CA – California; CO – Colorado; ID – Idaho; MB – Manitoba; MN – Minnesota; MT – Montana; ND – North Dakota; NT – Northwest Territories; NU – Nunavut; NV – Nevada; ON – Ontario; OR – Oregon; QC – Quebec; SK – Saskatchewan; UT – Utah; WA – Washington; YT – Yukon. [Color figure can be viewed at wileyonlinelibrary.com].
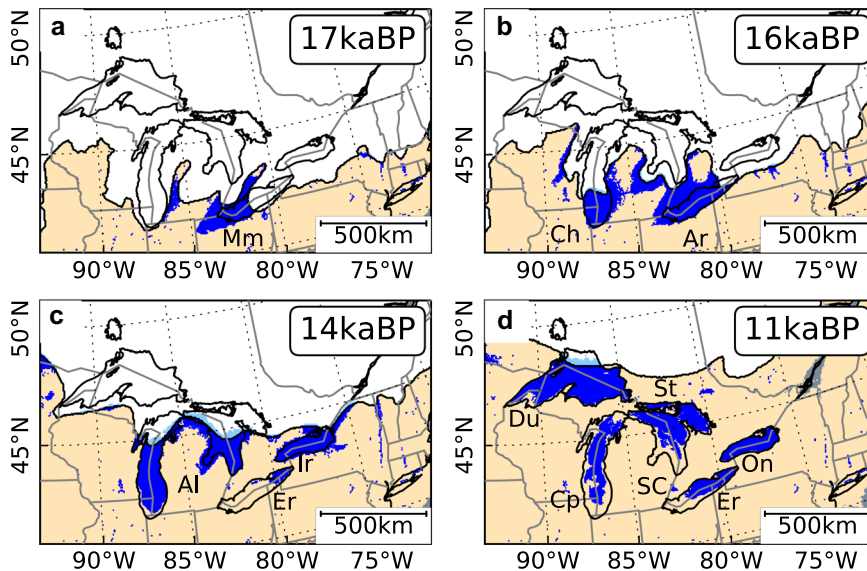
**Figure 4.** Formation of glacial lakes in the Great Lakes' basins for (a) 17 ka BP, (b) 16 ka BP, (c) 14 ka BP and (d) 11 ka BP. Black lines show the PD coastline and present major lakes. Lake names are abbreviated as follows: Al – Algonquin, Ar – Arkona, Ch – Chicago, Cp – Chippewa, Du – Duluth, Er – (Early) Erie, Ir – Iroquis, Mm – Maumee, On – (Early) Ontario, SC – St. Clair, St – Stanley. [Color figure can be viewed at wileyonlinelibrary.com].

(LakeCC) and measurements (CCGL). Since Lakes Huron and Michigan form a connected hydrological system, they are treated as a single lake. For all lakes, the reconstructed water level is close, but below the measured level, except for Lake Huron–Michigan, which is slightly overestimated. The same is true for the lake volume. Deviations in volume and surface area are between 1-4%, except for the relatively shallow Lake Erie, where the difference in volume is ~80 km$^3$ (~16% different). The total area and volume of the Great Lakes are underestimated by 2.2% and 1.6%, respectively. Lake St. Clair is located north of Lake Erie's western end. Due to its size it is usually not counted among the Great Lakes and is not highlighted by its outline here. However, the reconstruction fits well with the actual lake geometry (see Fig. 5).
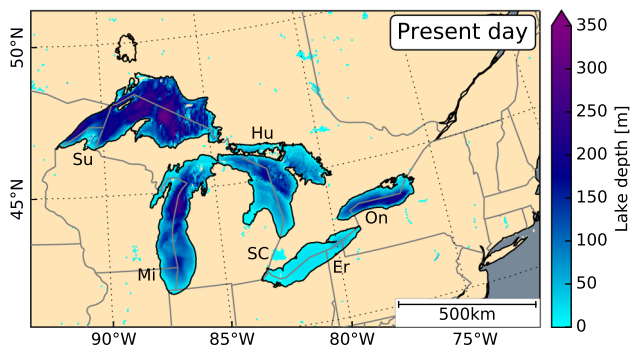


**Figure 5.** PD reconstruction of the Great Lakes. The blueish colours show lake depth, black lines depict the PD coastline and present major lakes. Lake names are abbreviated as follows: Er – Erie, Hu – Huron, Mi – Michigan, On – Ontario, SC – St. Clair, Su – Superior. [Color figure can be viewed at wileyonlinelibrary.com].

## Great Basin

The Great Basin is located between the Rocky Mountains and the Sierra Nevada, mainly in Nevada, Utah and California (see rectangle 4 in Fig. 3). Although the ice margin never extended this far south during the time span of interest, this region is treated here because the mountainous terrain has several lake basins.

The lake reconstructions show the formation of huge lakes in this area for every time slice; see Fig. 6a and overview maps (Fig. S2A–V). In Fig. 6a the red outlines mark the maximum extent of Lake Bonneville (Chen and Maloof, 2017), the predecessor of the Great Salt Lake, and Lake Lahontan (Reheis, 1999b), which covered the Black Rock Desert. These outlines match quite well with the reconstructed lake extents. Apart from these two lakes, the reconstruction also shows other filled valleys: the long lake parallel to the border between Nevada and California filling up Death Valley coincides with Lake Manly (compare with Blackwelder (1933) and the lacustrine sediments shown in Fig. 3). Also, the canyons cut by the Colorado River in southeastern Utah are filled up.

## Central North

At the LGM the southern margins of the Laurentide and Cordilleran ice sheets were located in central Montana (Dyke, 2004), along which several small lakes formed, as can be seen in Fig. 6b (this region corresponds to rectangle 2 in Fig. 3). The red outline shows the maximum extent of Lake Missoula (Pardee, 1910; Hanson et al., 2012). This lake, however, is not captured in the reconstruction; only small separate lakes fill up in this basin. The locations of the small lakes east of Lake Missoula along the ice margin are in good
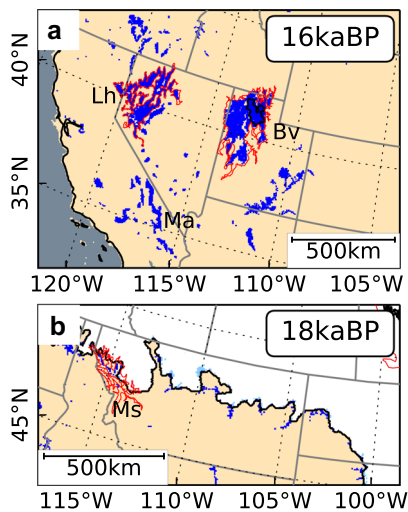
**Table 1.** Properties of PD reconstruction of the Great Lakes (LakeCC) compared with measurements (CCGL) (Coordinating Committee on Great Lakes Basic Hydraulic and Hydrologic Data, 1977).

| Lake | Area [km²] | | Volume [km³] | | Level [m] | | Max. depth [m] | |
|---|---|---|---|---|---|---|---|---|
| | LakeCC | CCGL | LakeCC | CCGL | LakeCC | CCGL | LakeCC | CCGL |
| Huron–Michigan | 116 075 | 117 400 | 8 493.1 | 8 460 | 177.0 | 176 | 266.3 | 281 |
| Superior | 79 600 | 82 100 | 11 762.4 | 12 100 | 177.0 | 183 | 360.7 | 405 |
| Erie | 24 700 | 25 700 | 405.0 | 484 | 171.2 | 174 | 59.0 | 64 |
| Ontario | 18 475 | 18 960 | 1 665.2 | 1 640 | 74.2 | 75 | 222.1 | 244 |
| **Total** | 238 850 | 244 160 | 22 325.7 | 22 684 | | | | |

**Figure 6.** (a) Lakes forming in the Great Basin region for 16 ka BP. Black line depicts the present coastline and today's major lakes (here: Great Salt Lake), the red line shows the maximum extent of the Pleistocene lakes Lahontan (Lh) and Bonneville (Bv). Lake Manly (Ma) is also labelled. (b) Several small lakes form along the ice margin in Montana at 18 ka BP. The red line depicts the maximum extent of glacial Lake Missoula (Ms) (Hanson *et al.*, 2012). [Color figure can be viewed at wileyonlinelibrary.com].

agreement with lakes reported by Davis *et al.* (2006), such as Lakes Musselshell, Winifred, Jordan and Glendive.

Fig. 7a shows an overview of the central north of North America at 15 ka BP. In this time slice, the LIS and CIS are about to separate. The reconstruction predicts the formation of huge lakes with a total volume of about 118 000 km$^3$ of freshwater in areas that just deglaciated in this time slice. For these lakes, however, no geological evidence is available. Due to lack of a name, these are called X and Y here. On the southern end of the LIS, the ice retreated far enough to expose parts of Lake Agassiz's basin. This newly formed lake fits quite well into the proposed margin of Teller and Leverington (2004). The small lake west of Lake Agassiz coincides well with Lake Souris (Kehew and Teller, 1994; Sun and Teller, 1997).

In Fig. 7b, the reconstruction of this region for 13 ka BP is shown. In the northwest, the retreating LIS exposed the Great Bear Lake basin, which contains glacial Lake McConnell. Where lake Y was previously, two much smaller lakes are found: Lake Meadow and Lake Saskatchewan (Christiansen, 1979; Kehew and Teller, 1994). In northwestern Alberta, Lake Peace (Hickin *et al.*, 2015) formed.

Table 2 contains surface area, volume, maximum depth, and the sink of the major lakes found in this region for the time between 15 ka BP and 9 ka BP. Lake Agassiz is found to drain towards the south until 12 ka BP (see Fig. 7c). In this time slice, the retreating ice margin exposed the basin of Lake McKenzie and parts of Lake McConnell's basin. Lake McConnell fits nicely into the basin reported by Smith (1994), but Lake McKenzie does not fill up except for a few separate cells.

Fig. 7d shows the reconstruction for 11 ka BP. The LIS retreated so far that a new drainage route for Lake Agassiz opened towards the Arctic (Table 2). The lake followed the ice margin and thus nearly doubled in size. It stays inside its proposed margin of maximum extent (Teller and Leverington, 2004), as does Lake McConnell (Smith, 1994).

At 10 ka BP (Fig. 7e) the ice margin in the west has not changed much compared with the previous time slice, but the margin in the south and southwest has retreated several hundreds of kilometres and the overall ice volume decreased. Lake Agassiz reaches its maximum size for the snapshots analysed here by almost doubling its volume once

again (see Table 2). In this configuration, it is draining towards the south. Lake McConnell's size decreased, and is split into separate basins.

In Fig. 7f (9 ka BP), the southern margin of the LIS rapidly retreated northward. This opens a new basin in the east for Lake Ojibway, which fits into the maximum outline of the Lake Agassiz/Ojibway basin. It appears twice in Table 2 because the two parts in Fig. 7f are not connected. Lake Agassiz is dramatically reduced in extent. Both lakes drain via the St. Lawrence River into the North Atlantic. This is the last time slice with major proglacial lakes appearing. At 8 ka BP, the LIS over Hudson Bay collapsed and overall dramatically decreased in size.

## Discussion

### Testing the LakeCC method

To validate the LakeCC model, the PD reconstructions of the Great Lakes are discussed in more detail. The reconstructed lake extent fits nicely with the actual shorelines (see Fig. 5) and also compares well with measurements (Coordinating Committee on Great Lakes Basic Hydraulic and Hydrologic Data, 1977) shown in Table 1. It should be noted that part of the difference is because different lake bathymetry data sets were used. However, we assume that this contribution is minor. The approximately 2% deviation in total area and volume are assumed to be due to the relatively coarse 5 km resolution. Deviation in water level is related to resolution that prevents the drainage route from being properly resolved. This issue results in small shallow lakes forming and can only be overcome by applying a minimum-filter to the high-resolution map, as was described above. This yields good results: major lakes are retained, while most unresolved valleys are drained. However, this comes at the cost of also draining lakes in narrow valleys that were actually existing, such as Lake Missoula (Fig. 6b) or Lake McKenzie (Fig 7b–f). Fig. 6a and the overview maps (Fig. S2A–V) show that the lakes in southeastern Utah experienced only minor changes in time due to GIA. Topography reconstructions in this area are therefore similar to the PD reference topography. As the canyons are drained by the Colorado River, we assume that the lakes in our reconstruction are artefacts originating from the coarse resolution.

The LakeCC tool basically only determines lake basins. How these are interpreted is up to the user. In this study, these lake basins are assumed to be filled to the top, for simplicity, but also because of a lack of any further information, such as climate and a temporally higher resolved glacial history. This simple assumption seems to be valid along the ice margins at times of glacial retreat. Examples for this issue being a problem in this study are the presence of Lake Bonneville (the predecessor of the Great Salt Lake), Lake Lahontan (in the Black Rock Desert) and Lake Manly (in Death Valley) at each time slice (see above). These are located in the Great Basin, which at present is the largest endorheic basin in North America and is characterised by an arid climate. The climatic conditions in this area were different in the past, as strandlines and lake sediments provide evidence of large ancient lakes (Chen and Maloof, 2017). These are assumed to have evaporated as the climate became drier (Reheis, 1999a). The reconstructed lakes, however, fit well within the outlines of maximum extent (see Fig. 6a).

Despite these uncertainties, the reconstructions are quite valuable in the context of this study, as we were more interested in the formation of the major lakes along the ice margin. A more elaborate study design would require more detailed information that is not available for such palaeo-applications.
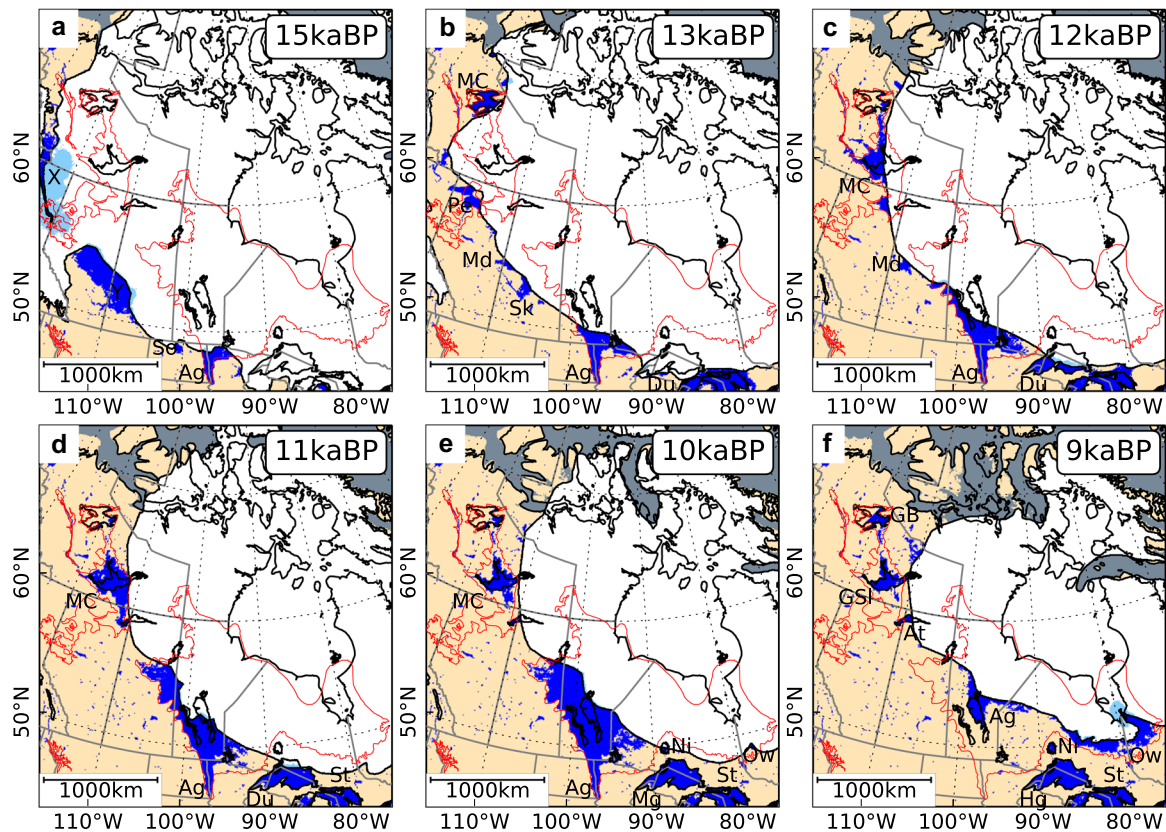
**Figure 7.** Overview of the North American central north at (a) 15, (b) 13, (c) 12, (d) 11, (e) 10, and (f) 9 ka BP. Black lines show the present-day coastline and major lakes, red lines show the maximum extent of major glacial lakes in this region. Lakes are labelled as follows: Ag – Agassiz, At – Athabasca, Du – Duluth, GB – Great Bear, GSl – Great Slave, Hg – Hughton, MC – McConnell, Md – Meadow, Mg – Minong, Ni – Nipigon, Ow – Ojibway, Pe – Peace, Sk – Saskatchewan, So – Souris, St – Stanley. Lakes X and Y have no real-world counterpart. See main text for more detail. [Color figure can be viewed at wileyonlinelibrary.com].

## Validation of the ice model

For this study, ice sheet and GIA reconstructions produced with the ICESHEET model (Gowan *et al.*, 2016a,b) were used to reconstruct lakes forming along the ice margin. This ice model was tuned to match various observations, such as GIA uplift rates, proglacial lake strandline tilt and relative sea level. One application of the present study is as a further indicator for the quality of the glacial reconstruction. As lake formation is quite sensitive to the ice margin location, the LakeCC model could be used to fine-tune ice margins in places where lakes form for which no geological evidence exists. Also, the water load should be included in the calculation of the GIA. This circular application is not done within this study; the lakes are rather used as a kind of benchmark to assess the glacial history of the ice sheet reconstruction.

One of those lakes without geological evidence is repeatedly forming between the LIS and CIS at around 60° N (see Fig. 7a), which, due to lack of a name, is called X in Table S1. It is present at the LGM (21 ka BP) but disappears again as the ice sheets merge at the beginning of the deglaciation. At 16 ka BP, the ice covering its basin has become thin enough that it fills again. The reason is that the Mackenzie River, which drains this region today, is fully glaciated. The lake disappears as this drainage route is open after 14 ka BP. Adjusting the ice margin of the LIS in this region a few kilometres to the east might solve this issue for 14 ka BP. For the earlier time slices this shift of the margin would be quite large. The reason why this basin did not fill up might simply be that the climatic conditions in this region were too cold.

The other lake is called Y in Table S1, and only forms between 15 and 14 ka BP at the southwestern margin of the LIS.

It is assumed that by shifting the ice margin southeast of this lake slightly to the northeast could drop the lake level about 200 m, which would almost drain the entire lake, leaving only small separate lakes, such as an early stage of Lake Peace at 14 ka BP in central Alberta (compare with Hickin *et al.* (2015) and the surficial sediments shown in Fig. 3).

Additionally, the model was applied to the ICE-6G_C reconstructions (Peltier *et al.*, 2015). As results are sensitive to the ice margin, the roughly resolved ice sheet was interpolated onto a higher resolved grid and cropped according to the ice margins used for the creation of ICE-6G_C (Dyke *et al.*, 2002, 2003).

Compared with the reconstructions of the NAICE model (Gowan *et al.*, 2016b) ICE-6G_C has more ice. This, in addition to the fact that a different Earth model structure was used, explains the deeper depression of the surface, which can be seen in the lake reconstructions. Fig. 8 shows the lake reconstruction for 12 ka BP; all other time slices can be found in S2 (Fig. S2A-V). The southern tip of Lake Agassiz in Fig. 8 is north of the Moorhead Low margin, that occurred at about that time (Breckenridge, 2015). The western margin merges with Lake McConnell and Lake McKenzie to form an enormous lake. The basins of the Great Lakes appear strongly tilted northward, with only small lakes forming in the basins of Lake Michigan and Lake Erie. Lake Ontario merged with the Champlain Sea.

## Drainage routes

Input of freshwater into the ocean at certain key regions can disrupt the thermohaline circulation and thus impact the global climate system (e.g. Manabe and Stouffer, 1997;

**Table 2.** Overview of the major glacial lakes in the Central North of North America between 15 ka BP and 9 ka BP.

| Time [ka BP] | Lake | Area [km²] | Volume [km³] | Max. depth [m] | Sink |
|---|---|---|---|---|---|
| 15 | Agassiz | 39 325 | 1 503.9 | 112.5 | South |
| | Souris | 4 225 | 59.4 | 34.2 | South |
| 14 | Agassiz | 78 375 | 4 549.1 | 152.4 | South |
| | McConnell | 24 200 | 927.5 | 77.3 | Arctic |
| | Hind | 2 650 | 42.9 | 82.8 | South |
| | McKenzie | 725 | 23.1 | 61.1 | Arctic |
| 13 | Agassiz | 85 950 | 4 973.3 | 152.1 | South |
| | McConnell | 32 975 | 1 383.6 | 96.9 | Arctic |
| | Peace | 27 850 | 1 675.1 | 178.2 | Arctic |
| | Saskatchewan | 13 925 | 462.1 | 125.7 | South |
| | Meadow | 6 800 | 212.4 | 99.5 | South |
| 12 | Agassiz | 147 175 | 10 265.3 | 181.2 | South |
| | McConnell | 60 925 | 3 704.3 | 132.9 | Arctic |
| | Meadow | 8 550 | 249.5 | 88.1 | South |
| 11 | Agassiz | 227 325 | 17 129.0 | 193.2 | Arctic |
| | McConnell | 94 975 | 4 638.5 | 158.8 | Arctic |
| 10 | Agassiz | 349 100 | 30 574.8 | 217.9 | South |
| | McConnell | 57 675 | 1 821.0 | 122.1 | Arctic |
| | Ojibway | 1 250 | 23.6 | 40.8 | St. Lawrence |
| 9 | Ojibway | 64 300 | 11 572.3 | 412.1 | St. Lawrence |
| | Agassiz | 60 650 | 1 226.1 | 87.2 | St. Lawrence |
| | Ojibway 2 | 40 700 | 2 123.1 | 167.3 | St. Lawrence |
| | Great Bear | 14 325 | 156.3 | 29.1 | Arctic |

Lohmann and Schulz, 2000; Kageyama *et al.*, 2009; Condron and Winsor, 2012). Broecker *et al.* (1989) proposed that the rerouting of LIS meltwater away from the southern spillway via the Mississippi River towards the east via the St. Lawrence Stream might have caused the onset of the Younger Dryas (YD). The diversion of drainage is consistent with a $\delta^{18}O$ anomaly measured in sediment cores from the Gulf of Mexico, which was caused by a sudden lack of freshwater input at the beginning of the YD (~12.9 ka BP) (Wickert *et al.*, 2013). However, there is still debate as to whether this rerouting of

Lake Agassiz overflow happened towards the east (Carlson *et al.*, 2007; Wickert *et al.*, 2013; Leydet *et al.*, 2018) or towards the Arctic via the Mackenzie River (Murton *et al.*, 2010; Keigwin *et al.*, 2018). These different drainage routes are marked as green arrows in Fig. 3.

Applying the post-processing described above to our LakeCC reconstructions we estimated the drainage routes and affected ocean basins for Lake Agassiz (see Table 2). From the first appearance of Lake Agassiz at 15 ka BP it overflows at its southern end and drains via the Mississippi River into the
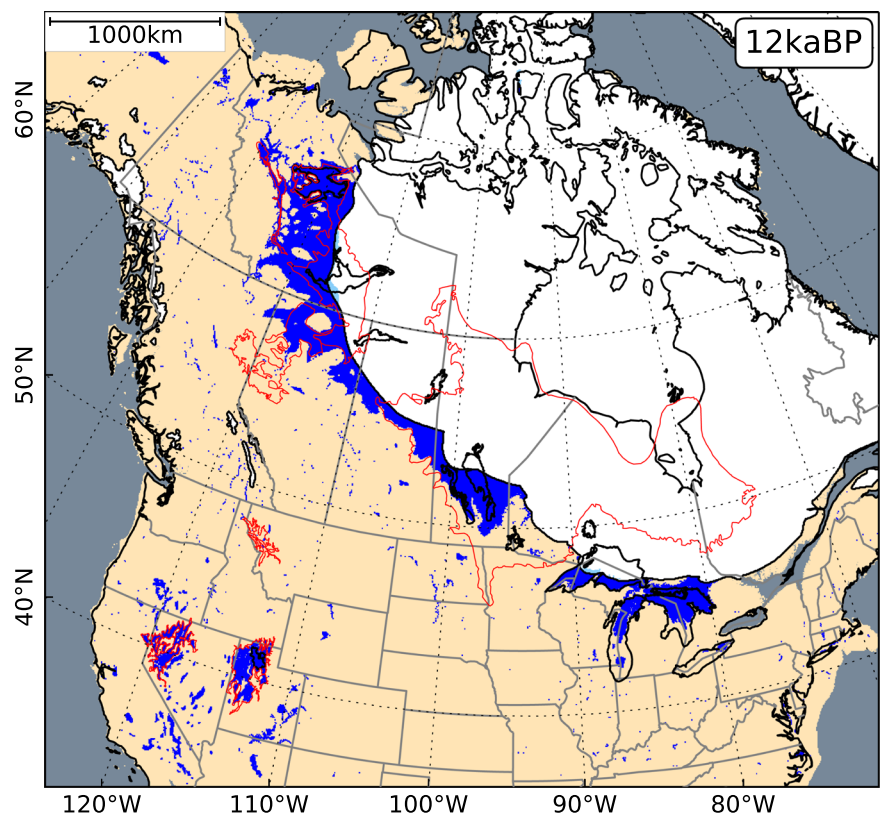


**Figure 8.** This map gives an overview of the lake reconstructions in North America at 12 ka BP using the ICE-6G_C ice and palaeogeographic reconstruction (Peltier *et al.*, 2015) [Color figure can be viewed at wileyonlinelibrary.com].

Gulf of Mexico. At the beginning of the YD at 13 ka BP (Fig. 7b) the northern half of Saskatchewan is still covered by thick ice, as is the northern half of the Great Lakes (see Fig. S2Ia). This prevents the lake draining to the north and east. The southern drainage route in our reconstructions is active until 12 ka BP, after the onset of the YD. These results neither support, nor refute any of these drainage scenarios, as the lake outlets depend strongly on an accurate reconstruction of the ice margin. The southeastern LIS margin used for the NAICE reconstruction (Gowan et al., 2016b) resembles the ice margin by Dyke (2004), i.e. recent discoveries about the timing of ice retreats (e.g. Leydet et al., 2018) are not accounted for. Furthermore, due to the coarse temporal resolution of the ice sheet reconstruction (1 ka), advances and retreats of ice lobes are not resolved. The ice margin blocking the northwestern drainage route does not necessarily contradict the freshening of the Beaufort Sea at the beginning of the YD, as reported by Keigwin et al. (2018). The source of this signal can be attributed to the rapid deglaciation of the northwestern LIS (Tarasov and Peltier, 2005, 2006) and drainage events of other major proglacial lakes in this region, such as Lake McConnell or Lake Peace (Wickert, 2014, 2016).

Breckenridge (2015) dated the palaeostrandline of Lake Agassiz that is associated with the opening of a lower spillway towards the north to 12.18 ± 0.48 ka BP. This happens in our reconstructions at 11 ka BP, when the northwestern part of the LIS has retreated far enough to open a new gateway to the Mackenzie River (see Fig. 7d). The outlets to the north and south do not differ much in height, as the southwestern shoreline of Lake Agassiz barely changed compared with the previous time slice (Fig. 7c). At 10 ka BP (Fig. 7e) the northward drainage route has closed again, possibly due to GIA, and drainage is again via the Mississippi River. The re-activation of the Mississippi drainage route is consistent with Wickert (2014). As already mentioned before, the exact timing is sensitive to the ice margin positions, which are often poorly constrained. Especially dynamic processes, such as advances and retreats of ice lobes, are only poorly covered.

Before Lake Agassiz finally drains around 8 ka BP as the LIS over Hudson Bay breaks apart, a new drainage route via Lake Ojibway to the St. Lawrence River appears (9 ka BP, Fig. 7f). In our reconstruction, the opening of this spillway yields an extreme drop in lake level. The diversion of flow away from Lake Superior towards Lake Ojibway can be found in sedimentary records and is dated to ~9.04 ka BP (Breckenridge et al., 2004, 2012; Wickert, 2014).

## Conclusions

In this study we have presented a tool to efficiently locate closed basins for a given palaeotopography configuration. After pre-processing the topography data set, we are able to retrieve lake reconstructions that, despite the relatively coarse grid, are in good agreement with geological data. For PD, the reconstructed Great Lakes lake volume, surface area and water levels agree well with observations. The LakeCC model was also applied to palaeoreconstructions of ice and GIA from the NAICE (Gowan et al., 2016b) and ICE-6G (Peltier et al., 2015) models. The results show the evolution of major glacial lakes, such as Lake Agassiz, Lake McConnell and the various predecessors of the Great Lakes. The discrepancy between reconstruction and geological data was used to infer places where the ice margin and volume might need adjustments.

The LakeCC model can be used to improve the ice sheet and topography reconstructions by applying adjustments of the ice margin and ice volume, and by adding the water load of the lakes into the calculation of the GIA. Furthermore, the model results give an idea about deglacial meltwater distribution, which is an important factor in the global climate system. In a future study we will couple the LakeCC model to an ice sheet model and investigate the impact of lakes on ice dynamics.

## Supporting information

Additional supporting information may be found in the online version of this article at the publisher's web-site.

S1 Table containing area, volume, lake level, maximum depth,and sink for all identified lakes

S2 Overview maps of the lake reconstructions (for both, NAICE and ICE-6G) in North America for different time slices

## Code availability

The code of the LakeCC model and the post-processing tools are available online in S. Hinck's *GitHub* repository (https://github.com/sebhinck). Both tools are archived at https://doi.org/10.5281/zenodo.3533070 and https://doi.org/10.5281/zenodo.3533050, respectively.

## Competing interests

The authors declare that they have no conflicts of interest.

## References

Barber DC, Dyke A, Hillaire-Marcel C et al. 1999. Forcing of the cold event of 8,200 years ago by catastrophic drainage of Laurentide lakes. *Nature* **400**(6742): 344.

Barnes R. 2016. Parallel Priority-Flood depression filling for trillion cell digital elevation models on desktops or clusters. *Computers & Geosciences* **96**: 56–68. https://doi.org/10.1016/j.cageo.2016.07.001

Barnes R, Lehman C, Mulla D. 2014. Priority-flood: An optimal depression-filling and watershed-labeling algorithm for digital elevation models. *Computers & Geosciences* **62**: 117–127. https://doi.org/10.1016/j.cageo.2013.04.024

Barnes R, Callaghan KL, Wickert AD. 2019. Computing water flow through complex landscapes, Part 2: Finding hierarchies in depressions and morphological segmentations. *Earth Surface Dynamics Discussions,* https://doi.org/10.5194/esurf-2019-34

Batchelor CL, Margold M, Krapp M et al. 2019. The configuration of Northern Hemisphere ice sheets through the Quaternary. *Nature Communications* **10**(1): 1–10.

Berends CJ, van de Wal RSW. 2016. A computationally efficient depression-filling algorithm for digital elevation models, applied to proglacial lake drainage. *Geoscientific Model Development* **9**(12): 4451–4460.

Börck S. 1995. A review of the history of the Baltic Sea, 13.0-8.0 ka BP. *Quaternary International* **27**: 19–40, https://doi.org/10.1016/1040-6182(94)00057-C

Blackwelder E. 1933. Lake Manly: An Extinct Lake of Death Valley. *Geographical Review* **23**(3): 464. https://doi.org/10.2307/209632

Breckenridge A. 2013. An analysis of the late glacial lake levels within the western Lake Superior basin based on digital elevation models. *Quaternary Research* **80**(3): 383–395. https://doi.org/10.1016/j.yqres.2013.09.001

Breckenridge A. 2015. The Tintah-Campbell gap and implications for glacial Lake Agassiz drainage during the Younger Dryas cold interval. *Quaternary Science Reviews* **117**: 124–134. https://doi.org/10.1016/j.quascirev.2015.04.009

Breckenridge A, Johnson TC, Beske-Diehl S et al. 2004. The timing of regional Lateglacial events and post-glacial sedimentation rates from Lake Superior. *Quaternary Science Reviews* **23**(23): 2355–2367. https://doi.org/10.1016/j.quascirev.2004.04.007

Breckenridge A, Lowell TV, Stroup JS et al. 2012. A review and analysis of varve thickness records from glacial Lake Ojibway (Ontario and Quebec, Canada). *Quaternary International* **260**: 43–54. https://doi.org/10.1016/j.quaint.2011.09.031

Bretz JH. 1923. The Channeled Scablands of the Columbia Plateau. *The Journal of Geology* **31**(8): 617–649. https://doi.org/10.1086/623053

Broecker WS. 2006. Was the Younger Dryas Triggered by a Flood? *Science* **312**(5777): 1146–1148.

Broecker WS, Kennett JP, Flower BP et al. 1989. Routing of meltwater from the Laurentide Ice Sheet during the Younger Dryas cold episode. *Nature* **341**(6240): 318.

Carlson AE, Clark PU. 2012. Ice sheet sources of sea level rise and freshwater discharge during the last deglaciation. *Reviews of Geophysics* **50**(4): RG4007.

Carlson AE, Clark PU, Haley BA et al. 2007. Geochemical proxies of North American freshwater routing during the Younger Dryas cold event. *Proceedings of the National Academy of Sciences* **104**(16): 6556–6561.

Chen CY, Maloof AC. 2017. Revisiting the deformed high shoreline of Lake Bonneville. *Quaternary Science Reviews* **159**: 169–189. https://doi.org/10.1016/j.quascirev.2016.12.019

Christiansen EA. 1979. The Wisconsinan deglaciation, of southern Saskatchewan and adjacent areas. *Canadian Journal of Earth Sciences* **16**(4): 913–938.

Condron A, Winsor P. 2012. Meltwater routing and the Younger Dryas. *Proceedings of the National Academy of Sciences* **109**(49): 19928–19933.

Coordinating Committee on Great Lakes Basic Hydraulic and Hydrologic Data. 1977. *Coordinated Great Lakes physical data*. Coordinating Committee on Great Lakes Basic Hydraulic and Hydrologic Data, Chicago, IL and Cornwall, ON. URL https://www.lre.usace.army.mil/Portals/69/docs/GreatLakesInfo/docs/CoordinatedGreatLakesPhysicalData/CoordinatedGreatLakesPhysicalData-May1977-MediumRes.pdf

Davis NK, Locke WW, Pierce KL et al. 2006. Glacial Lake Musselshell: Late Wisconsin slackwater on the Laurentide ice margin in central. *Montana, USA. Geomorphology* **75**(3): 330–345.

Dyke AS. 2004. An outline of North American deglaciation with emphasis on central and northern Canada, *Developments in Quaternary Sciences*. Elsevier, 373–424. https://doi.org/10.1016/S1571-0866(04)80209-4

Dyke AS, Andrews JT, Clark PU et al. 2002. The Laurentide and Innuitian ice sheets during the Last Glacial Maximum. *Quaternary Science Reviews* **21**(1): 9–31.

Dyke AS, Moore A, Robertson L. 2003. Deglaciation of North America. *Technical Report* **1574**. https://doi.org/10.4095/214399

Fullerton DS, Bush CA, Pennell JN 2003. Map of surficial deposits and materials in the eastern and central United States (east of 102 degrees West longitude). USGS Numbered Series, U.S. Geological Survey. https://doi.org/10.3133/i2789

Geological Survey of Canada. 2014. Surficial geology of Canada. Technical Report 195. https://doi.org/10.4095/295462

Gowan EJ. 2013. An assessment of the minimum timing of ice free conditions of the western Laurentide Ice Sheet. *Quaternary Science Reviews* **75**: 100–113. https://doi.org/10.1016/j.quascirev.2013.06.001

Gowan EJ, Tregoning P, Purcell A et al. 2016a. ICESHEET 1.0: a program to produce paleo-ice sheet reconstructions with minimal assumptions. *Geoscientific Model Development* **9**(5): 1673–1682.

Gowan EJ, Tregoning P, Purcell A et al. 2016b. A model of the western Laurentide Ice Sheet, using observations of glacial isostatic adjustment. *Quaternary Science Reviews* **139**: 1–16. https://doi.org/10.1016/j.quascirev.2016.03.003

Hanson MA, Lian OB, Clague JJ. 2012. The sequence and timing of large late Pleistocene floods from glacial Lake Missoula. *Quaternary Science Reviews* **31**: 67–81. https://doi.org/10.1016/j.quascirev.2011.11.009

Hickin AS, Lian OB, Levson VM et al. 2015. Pattern and chronology of glacial Lake Peace shorelines and implications for isostacy and ice-sheet configuration in northeastern British Columbia, Canada. *Boreas* **44**(2): 288–304.

Kageyama M, Mignot J, Swingedouw D et al. 2009. Glacial climate sensitivity to different states of the Atlantic Meridional Overturning Circulation: results from the IPSL model. *Climate of the Past* **5**(3): 551–570.

Kehew AE, Teller JT. 1994. History of late glacial runoff along the southwestern margin of the Laurentide Ice Sheet. *Quaternary Science Reviews* **13**(9): 859–877.

Keigwin LD, Klotsko S, Zhao N et al. 2018. Deglacial floods in the Beaufort Sea preceded Younger Dryas cooling. *Nature Geoscience* **11**(8): 599.

Khosravi S 2017. Comparison of the Past Climate in Northern Canada and Greenland. Master's thesis, University of Bremen, Bremen, Germany. URL http://www.iup.uni-bremen.de/PEP_master_thesis/thesis_2017/Khosravi_Sara_MScThesis.pdf

Khroulev C 2017. An implementation of a standard 2-scan connected component labeling algorithm using run-length encoding: ckhroulev/connected-components. URL https://github.com/ckhroulev/connected-components. Last access: 9 January 2019.

Lambeck K, Purcell A, Zhao J et al. 2010. The Scandinavian Ice Sheet: from MIS 4 to the end of the Last Glacial Maximum. *Boreas* **39**(2): 410–435.

Larsen CE 1988. Geological history of glacial Lake Algonquin and the upper Great Lakes. USGS Numbered Series 1801, U.S. G.P.O. URL http://pubs.er.usgs.gov/publication/b1801

Lewis C, Moore TC, Rea DK et al. 1994. Lakes of the Huron basin: their record of runoff from the laurentide ice sheet. *Quaternary Science Reviews* **13**(9-10): 891–922.

Lewis CFM, Anderson TW. 1989. Oscillations of levels and cool phases of the Laurentian Great Lakes caused by inflows from glacial Lakes Agassiz and Barlow-Ojibway. *Journal of Paleolimnology* **2**(2): 99–146.

Leydet DJ, Carlson AE, Teller JT et al. 2018. Opening of glacial Lake Agassiz's eastern outlets by the start of the Younger Dryas cold period. *Geology* **46**(2): 155–158.

Lohmann G, Schulz M. 2000. Reconciling Bølling Warmth with peak deglacial meltwater discharge. *Paleoceanography* **15**(5): 537–540.

Manabe S, Stouffer RJ. 1997. Coupled ocean-atmosphere model response to freshwater input: Comparison to Younger Dryas Event. *Paleoceanography* **12**(2): 321–336.

Mathews WH 1980. Retreat of the last ice sheets in northeastern British Columbia and adjacent Alberta. Technical Report 331. https://doi.org/10.4095/102160

Murton JB, Bateman MD, Dallimore SR et al. 2010. Identification of Younger Dryas outburst flood path from Lake Agassiz to the Arctic Ocean. *Nature* **464**(7289): 740–743.

Pardee JT. 1910. The Glacial Lake Missoula. *The Journal of Geology* **18**(4): 376–386.

Pardee JT. 1942. Unusual currents in Glacial Lake Missoula, Montana. *GSA Bulletin* **53**(11): 1569–1600.

Peltier WR, Argus DF, Drummond R. 2015. Space geodesy constrains ice age terminal deglaciation: The global ICE- 6G C (VM5a) model. *Journal of Geophysical Research: Solid Earth* **120**(1): 450–487.

Reheis M. 1999a. Highest Pluvial-Lake Shorelines and Pleistocene Climate of the Western Great Basin. *Quaternary Research* **52**(2): 196–205.

Reheis MC 1999b. Extent of Pleistocene lakes in the western Great Basin. USGS Numbered Series 2323. URL http://pubs.er.usgs.gov/publication/mf2323

Schaffer J, Timmermann R, Arndt JE et al. 2016. A global, high-resolution data set of ice sheet topography, cavity geometry, and ocean bathymetry. *Earth System Science Data* **8**(2): 543–557.

Smith DG. 1992. Glacial Lake Mackenzie, Mackenzie Valley, Northwest Territories, Canada. *Canadian Journal of Earth Sciences* **29**(8): 1756–1766.

Smith DG. 1994. Glacial Lake McConnell: Paleogeography, age, duration, and associated river deltas, Mackenzie River basin, western Canada. *Quaternary Science Reviews* **13**(9): 829–843.

Soller DR, Reheis MC, Garrity CP *et al.* 2009. Map Database for Surficial Materials in the Conterminous United States. URL https://pubs.usgs.gov/ds/425/

Sun CS, Teller JT. 1997. Reconstruction of glacial Lake Hind in southwestern Manitoba, Canada. *Journal of Paleolimnology* **17**(1): 9–21.

Tarasov L, Peltier W. 2005. Arctic freshwater forcing of the Younger Dryas cold reversal. *Nature* **435**(7042): 662–665.

Tarasov L, Peltier WR. 2006. A calibrated deglacial drainage chronology for the North American continent: evidence of an Arctic trigger for the Younger Dryas. *Quaternary Science Reviews* **25**(7–8): 659–688.

Taylor FB. 1915. Glacial Lake Whittlesey, *The Pleistocene of Indiana and Michigan, History of the Great Lakes, volume 53 of Monographs of the United States Geological Survey*. U.S. Government Printing Office: Washington, D.C.

Teller JT, Leverington DW. 2004. Glacial Lake Agassiz: A 5000 yr history of change and its relationship to the δ18 O record of Greenland. *Geological Society of America Bulletin* **116**(5-6): 729–742.

The PISM authors. 2015. PISM, a Parallel Ice Sheet Model. URL http://www.pism-docs.org/. Last access: 9 January 2019.

Tweed FS, Carrivick JL. 2015. Deglaciation and proglacial lakes. *Geology Today* **31**(3): 96–102.

Waitt RB. 1985. Case for periodic, colossal jökulhlaups from Pleistocene glacial Lake Missoula. *Geological Society of America Bulletin* **96**(10): 1271. https://doi.org/10.1130/0016-7606(1985) 962.0.CO;2

Walder JS, Trabant DC, Cunico M *et al.* 2006. Local response of a glacier to annual filling and drainage of an ice-marginal lake. *Journal of Glaciology* **52**(178): 440–450.

Wickert AD. 2014. Impacts of Pleistocene glaciation and its Geophysical Effects on North American River Systems. *Geological Sciences Graduate Theses & Dissertations* 79.

Wickert AD. 2016. Reconstruction of North American drainage basins and river discharge since the Last Glacial Maximum. *Earth Surface Dynamics* **4**(4): 831–869.

Wickert AD, Mitrovica JX, Williams C *et al.* 2013. Gradual demise of a thin southern Laurentide ice sheet recorded by Mississippi drainage. *Nature* **502**(7473): 668–671.

Wu Q, Lane CR. 2016. Delineation and Quantification of Wetland Depressions in the Prairie Pothole Region of North Dakota. *Wetlands* **36**(2): 215–227.

Wu Q, Liu H, Wang S *et al.* 2015. A localized contour tree method for deriving geometric and topological properties of complex surface depressions based on high-resolution topographical data. *International Journal of Geographical Information Science* **29**(12): 2041–2060.